Effects of surface roughness on the electronic shell structure of metal clusters

J. Lermé, M. Pellarin, E. Cottancin, B. Baguenard, J. L. Vialle, and M. Broyer
Laboratoire de Spectrométrie Ionique et Moléculaire, CNRS and Université Lyon I, Bâtiment 205, 43 Boulevard du 11 Novembre 1918, 69622 Villeurbanne Cedex, France
(Received 10 April 1995; revised manuscript received 13 July 1995)

Electronic shell and supershell structures in spherical metal clusters with a rough surface are quantum mechanically investigated. Our nonperturbative approach involves a finite-depth step-walled spherical potential well with a sine-wave corrugation along the azimuthal and polar angular coordinates. The electronic structure is studied as a function of both the radial amplitude and the angular wavelength of the corrugation. When the spatial periods of the roughness are comparable to, or shorter than the Fermi wavelength, the shell structure related to the overall spherical symmetry survives, even in the case of a large radial corrugation amplitude. The weakening of the shell effects due to the loss of the spherical symmetry is rather minor and the electronic structure is essentially ruled by the spherical average of the rough potential, which has a soft surface profile. In consequence, the magic sizes (supershell beat locations) are slightly (noticeably) shifted towards larger sizes. These shifts depend strongly on the radial roughness amplitude. As far as the electronic structure is concerned, the results establish the equivalence between a fine-grained hard-walled rough potential and a spherical potential having a soft surface profile. Hence surface roughness could underlie partly the shift of the supershell nodes observed in trivalent metal experiments. When the wavelengths of the corrugation along the angular coordinates are large relative to the Fermi one the electronic density of states becomes quite smooth owing to the large level splitting and mixing effects. The supershell pattern and—to a lesser extent—the shell structure are considerably damped, and even may disappear. In consequence the size dependence of the shell-correction energy and of the ionization potential do not exhibit noticeable oscillations, except for small radial roughness amplitudes.

I. INTRODUCTION

Since the pioneering paper by Knight *et al.*,[1] numerous works have been devoted to studying the electronic shell structure in metal clusters.[2–7] The structureless jellium model (JM),[8–11] usually worked out within the Kohn-Sham (KS) density-functional theory, explains successfully the major features of the observed electronic shell structure that results from the sequential filling of the $2(2l+1)$-fold degenerate KS levels $E_{n,l}$ by the N_e valence electrons. In the JM, the discrete ionic background is replaced by a spherical homogeneous hard-walled positive charge distribution of radius $R_{N_e}=r_s N_e^{1/3}$, where r_s is the Wigner-Seitz radius per valence electron in the bulk. Improvements of this simple model, by involving softer jellium walls,[12–16] or by taking into account accurate electron-ion interaction through local[17–19] or nonlocal[20–22] pseudopotentials, have brought the theory in better agreement with the experimental results. In including these model refinements the spherical symmetry and the homogeneity of the inner ionic density have been assumed (except in Ref. 21 where the discreteness of the ionic frame is preserved), thus ensuring practicability of the calculations even for very large cluster sizes. Concerning the cluster homogeneity, calculations involving strongly inhomogeneous clusters consisting of nested concentric spherical atomic layers, have shown that the smoothness of the background is not an essential theoretical constraint.[19] Thus, the overall spherical cluster shape seems to be the only requirement for the emergence of the observed electronic shell structure in liquid clusters (more exactly the possibility for the clusters of getting the spherical shape for magic sizes). Let us remark that the spherical-symmetry hypothesis was not assumed for computational convenience only. A crude perturbative analysis suggests that taking into account the angular-dependent component of the effective electronic potential gives rise to a weakening of the shell effects through the removal of the $(2l+1)$-fold orbital degeneracy ("level broadening" effect), but does not modify the magic numbers or supershell node locations.[19] Rightness of this analysis would provide insight into the validity of the JM, seeing that the electrostatic potential of the jellium distribution is actually a quite good numerical approximation for the spherically averaged electrostatic potential produced by a homogeneous spherical distribution of pointlike ions. Thus, usual justifications for the JM, consisting in invoking statistical arguments—ensemble or time averaging of the ionic distribution—would appear to be needless. Thus, apart from the overestimation of the shell effects due to the high level degeneracy, it seems that the Coulombic short-range behavior of the electron-ion interaction is actually the major approximation involved in the JM.

The main purpose of this paper is to study how, and to what extent, the electronic shell structure is modified when the angular-dependent component of the effective electronic potential is taken into account. In addition,

0163-1829/95/52(19)/14163(14)/$06.00

the quantum model calculations reported in this paper will test the spherical averaging approximation assumed in previous works for determining the magic sizes and the supershell beat locations. Throughout this paper, only the loss of the spherical symmetry due to the surface roughness will be investigated. Effects of surface roughness are expected to be of particular importance, because the surface profile of the electronic potential was found to be the major feature governing the electronic shell structure.[11,16–19,23] The study of the influence of the inner background granularity, which is expected to produce only a slight decrease of the shell-effects strength, is left for further work (the characteristic wavelength λ of the perturbation associated with the internal granularity, typically on the order of the average ion-ion distance, is slightly smaller than the Fermi wavelength $\lambda_f \approx 3.3 r_s$).

Works dealing explicitly with the effects of surface roughness, or including implicitly these effects, have already been published. We briefly review and discuss some of them. In the very low cluster-size domain, calculations taking into account the discrete background structure preserve—except for a noticeable weakening—the electronic shell structure as obtained in the spherical JM,[24–27] although defining an outer cluster shape is rather difficult, because the surface is highly rough on the cluster-size scale. In fact, for very small sizes, the gaps between the levels $E_{n,l}$ (levels obtained at the zeroth-order approximation for the electronic Hamiltonian, for instance, the ones provided by the JM) are large and the level splittings, due to the lattice structure effects, do not mix strongly the zeroth-order levels or bunches.[27] In the medium size range (say $N_e < 1000$), Hückel calculations of the electronic state density (DOS) in spherical or polyhedral fcc clusters have shown that the discreteness of the structure does not destroy the JM-like electronic structure in the lower region of the electronic spectrum.[28,29] However, beyond the sizes $N_e = 200$–400, depending on the cluster shape, JM-like DOS are never observed over a wide region surrounding the Fermi level, even for fcc clusters built to ensure the most perfectly the spherical shape. These results are inconsistent with the experimental results: for sodium and gallium clusters the JM-related electronic shell and supershell structures have been observed up to $N_e = 3000$ (Ref. 4) and 15 000 (Refs. 6 and 30) valence electrons, respectively. The disagreement could be due, either to the unsuitability of the tight-binding approach for describing large clusters, or to the constraint of using only fcc (or more generally bulk-lattice) sites to generate the cluster structure. To our knowledge, except a paper by Ratcliff,[31] a two-dimensional study by Barojas *et al.*,[32] and a very recent investigation by Pavloff,[33] which all involve a corrugated potential well to tackle the effects of surface roughness, the theoretical framework as well as the main purpose of most of the previous works[34–40] differ from ours. Briefly, these studies deal with clusters built from periodic bulklike lattices, and tight-binding Hamiltonians are assumed to calculate the electronic levels. The central task consists in determining the energy-level statistics from an ensemble of clusters having the same number of atoms but different surface shapes, in order to test the predictions of the random matrix theory, successfully applied in nuclear physics.[41] With regard to the works involving corrugated potential wells, Ratcliff describes the surface deformation of a spherical infinite-depth hard-walled potential box by a linear superposition of spherical harmonics, with coefficients randomly chosen from a Gaussian distribution in order to generate the ensemble.[31] However, a perturbative treatment is used, i.e., the surface distortion is diagonalized within a given zeroth-order $(2l+1)$-fold-degenerate subspace, and hence no information about the survival or the vanishing of the JM-like electronic shell structure can be gained in this work. Much more closely related to our investigation is the paper by Pavloff[33] in which the electronic DOS in infinite-depth hard-walled potential wells exhibiting small surface deformations from a perfect sphere is calculated. This study is carried out at a perturbative level (the deformations are assumed small) within the semiclassical theory. The DOS is then ensemble averaged over the surface disorder through a Gaussian distribution of the deformation parameter. Our quantum calculations are in disagreement with the results reported in Ref. 33. We think that part of the discrepancies are rooted in the deficiencies of the semiclassical trace formula approach, which basically assumes an infinitesimal Planck constant, and is therefore unsuitable for dealing with surface distortions having spatial scales comparable to or shorter than the Fermi wavelength.

The paper is organized as follows. In Sec. II, we detail the model assumed for investigating the surface corrugation effects, as well as the mathematical procedure used to calculate the eigenvalues in nonspherical rough potential wells. Obviously the effective electronic potential is not derived from self-consistent KS calculations involving optimized cluster structures. Nevertheless, we would like to stress that the qualitative results obtained with our simple model potentials, consisting of spherical finite-depth hard-walled potential wells with a sine-wave corrugation, are quite general and can be extrapolated to more realistic corrugated soft KS-electronic potentials. The changes in the electronic shell structure, due to the surface roughness, are analyzed by plotting, either electronic DOS curves, or the evolution of the shell-correction energy or of the ionization potential as a function of the cluster size. Specific effects of short-wavelength corrugation intrinsic to the background granularity (λ on the order of r_s), as well as of long-wavelength corrugation ($\lambda > r_s$), are studied for various amplitudes of the deformation relative to a perfect spherical shape. The results are reported in Sec. III. Concluding remarks and a summary of the major results are given in Sec. IV. Atomic units are used throughout this paper.

II. THE MODEL

A. Parametrization of the rough surface

The corrugated KS-effective electronic potential of real clusters is mimicked by a spherical finite-depth ($V_0 < 0$) step-walled potential well of radius R_{N_e} with a sine-curve deformation along the two angular coordinates. The

modulated surface of the rough well is assumed located, in the direction (θ,ϕ), at the distance

$$R(\theta,\phi)=R_{N_e}+A\cos(n_1\theta)\cos(n_2\phi)\ , \tag{1}$$

from the cluster center (see Fig. 1). A is the amplitude of the surface deformation $(R_{N_e}-A<R(\theta,\phi)<R_{N_e}+A)$, and n_1 and n_2 are two positive integers. We will take $n_1=n_2=n_{\rm cor}$ throughout this paper (cor means corrugation). This simple roughness parametrization does not ensure a homogeneous spatial corrugation over the whole surface. Equation (1) corresponds to two shifted square lattices of bumps and hollows near the equatorial region $(\theta=\pi/2)$, which progressively become more and more distorted as one approaches the two polar regions ($\theta=0$ and π). An immediate representation is provided by imaging the pattern formed by parallels and meridians, with the same angular spacing, drawn on a globe, symbolizing the lines of zero radial displacement between the successive bump and hollows $(R(\theta,\phi)=R_{N_e}$ for $n_{\rm cor}\theta$ or $n_{\rm cor}\phi=\pi/2[\mathrm{mod}\pi])$. Note that the square surface lattices form an angle equal to $\pi/4$, with the parallels and meridians. Let us stress that the parametrization Eq. (1), chosen for computational convenience in order to reduce the size of the matrixes to be diagonalized (see Secs. II B and II C), does not give rise to spurious specific effects. Indeed most of the results, except those related to the effective surface softness (Sec. III B), can be easily inferred by comparing the length scale of the corrugation with the Fermi wavelength. The qualitative conclusions drawn from our model calculations are then general. In our model the grain of the corrugation can be roughly characterized by the spatial period of the square lattices of bumps and hollows in the equatorial region $d_{\rm cor}=2^{-1/2}(2\pi R_{N_e}/n_{\rm cor})$.

B. The numerical procedure

The single-electron eigenvalues and eigenfunctions are obtained by solving the Schrödinger equation for the Hamiltonian $H=H_0+\Delta V(\mathbf{r})$. H_0 is the "unperturbed" Hamiltonian associated with the perfect spherical well of radius R_{N_e}: $H_0=-(\frac{1}{2})\Delta+V(r)$ with $V(r)=V_0\Theta(R_{N_e}-r)$. $\Delta V(\mathbf{r})$ is defined by

$$\Delta V(\mathbf{r})=V_0\{\Theta[R(\theta,\phi)-r]-\Theta(R_{N_e}-r)\}\ , \tag{2}$$

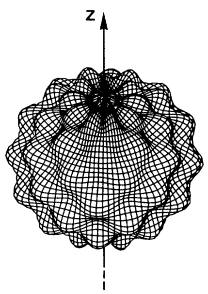

FIG. 1. The rough surface bounding the electronic potential well [$V(\mathbf{r})=V_0<0$ inside the surface, $V(\mathbf{r})=0$ outside]. The rough surface is parametrized according to Eq. (1).

where Θ is the Heaviside or step function. The three-dimensional Schrödinger equation corresponding to the corrugated potential well is solved by numerical diagonalization of the Hamiltonian matrix $\langle\psi_{n,l,m}|H|\psi_{n',l',m'}\rangle$ in a truncated basis of the "unperturbed" Hamiltonian H_0. Such a method was previously used in Ref. 42 for calculating electronic DOS in a potential well having icosahedral symmetry. However, preliminary calculations have shown that the approximations assumed in Ref. 42 are too drastic, and applicability of the method for our purpose requires prior improvements. These concern two essential features to be fulfilled: (i) Because of the loss of the spherical symmetry, each "unperturbed" state $\psi_{n,l,m}$ interacts with numerous states of lower and higher energies. Hence, the truncated basis has to include an energy domain above the Fermi level sufficiently large to correctly calculate the overall repulsion from the upper levels; (ii) since the radius $R(\theta,\phi)$ of the rough potential box exceeds R_{N_e} at the surface bumps, the basis set has to suitably span the radial region corresponding to this additional classically allowed region $(R_{N_e}<r<R_{N_e}+A)$. This requirement is poorly ensured by the H_0-bound states, which have a noticeable amplitude in the region $r<R_{N_e}$ only. Therefore, the lowest part of the positive-energy spectrum, i.e., the close continuum, has to be included in the selected basis. A third requirement, which is of more technical nature, concerns the fit of the "unperturbed" radial wave functions in the region of interest (around R_{N_e}), which would be too poorly mimicked by its linear approximation,[42] except for small amplitudes A.

In order to achieve these goals, the basis set has been generated by an Hamiltonian H_0' involving a double-well potential $[H_0'=-(\frac{1}{2})\Delta+V'(r)]$, where $V'(r)$ is defined as (see Fig. 2)

$$\begin{aligned} &V'(r)=V_0<0,\quad 0<r<R_{N_e}\ ,\\ &V'(r)=0,\quad R_{N_e}<r<R_{N_e}+\Delta\ ,\\ &V'(r)=V_1>0,\quad r>R_{N_e}+\Delta\ . \end{aligned} \tag{3}$$

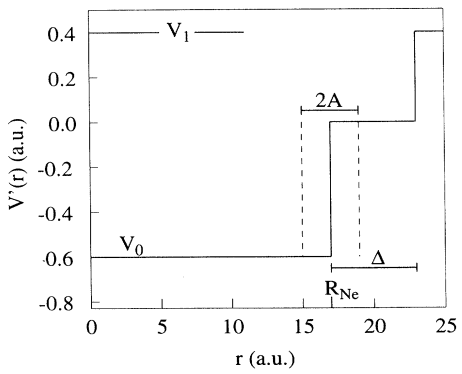

FIG. 2. The double-well spherical potential $V'(r)$ [Eq. (3)] used to generate the truncated basis set involved in the Hamiltonian-matrix diagonalization. $2A$ is the total radial amplitude of the sine-wave corrugation modulating the surface of the inner well.

The truncated basis (eigenstates $|\psi_{n,l,m}\rangle$, such as $E_{n,l}<V_1$) clearly fulfills both previous requirements for large enough values of the parameters Δ and V_1. H is split according to $H=H'_0+[V(r)-V'(r)]+\Delta V(\mathbf{r})$. The rigorous matrix elements $\langle\psi_{n,l,m}|H|\psi_{n',l',m'}\rangle$ are the sum of two contributions (except for the additional diagonal one $E_{n,l}\delta_{n,n'}\delta_{l,l'}\delta_{m,m'}$) involving the overlap of the wave functions over the radial domains $[R_{N_e}-A,R_{N_e}+A]$ [operator $\Delta V(\mathbf{r})$] and $[r>R_{N_e}+\Delta]$ [operator $V(r)-V'(r)$]. However, all the bound states of negative energy trapped in the central well have a vanishingly small amplitude beyond $r=R_{N_e}+\Delta$, and a simple perturbative analysis shows that the second contribution [matrix elements of $V(r)-V'(r)$] will have a negligible influence on the bound levels in the domain of interest ($E<E_f<0$). Strictly speaking, the approximation consisting in retaining only the matrix elements of $\Delta V(\mathbf{r})$ amounts to studying the roughness effects in the double-well potential, instead of in the original single-well one. Exact calculations (with no roughness) involving both potentials $V(r)$ and $V'(r)$ lead to identical energy levels of negative energy (for large enough values of Δ, the results are insensitive to the values of both parameters Δ and V_1). It is clear that this will hold true in the presence of the corrugation, and the convenient approximation made in disregarding the term $V(r)-V'(r)$ is numerically correct. Actually, the described procedure is closely related to the well-known technique used in molecular calculations, consisting in quantifying the continuum. Tests of the convergence of the results, versus Δ and V_1, have been carefully checked.

C. Matrix-element calculations

The eigenfunctions of H'_0 are expressed as

$$\Psi_{n,l,m}(\mathbf{r})=R_{n,l}(r)Y_{l,m}(\theta,\phi)\ , \tag{4}$$

where the functions $Y_{l,m}$ are the spherical harmonics and the radial functions $R_{n,l}(r)$ are linear combinations of spherical Bessel functions of the first and second kind, $j_l(z)$ and $y_l(z)$, respectively, with a real or imaginary argument, depending on the sign of $E-V'(r)$ ($z=kr$ or ikr, with $k=|2[E-V'(r)]|^{1/2}$). The matrix element of the perturbation $\Delta V(\mathbf{r})$,

$$\int_0^\infty\int_0^\pi\int_0^{2\pi}\psi^*_{n,l,m}(\mathbf{r})\Delta V(\mathbf{r})\times\psi_{n',l',m'}(\mathbf{r})r^2\sin(\theta)dr\,d\theta\,d\phi\ , \tag{5}$$

is transformed into a sum of products of one-dimensional integrals according to the following procedure. Each radial function $R_{n,l}(r)$ is beforehand replaced by a high-degree polynomial approximation in the radial domain of interest $R_{N_e}-A<r<R_{N_e}+A$, the coefficients of which are optimized by a least-square fit,

$$R_{n,l}(r)=\sum_{k=0}^{k_p}a_k(r-R_{N_e})^k\ . \tag{6}$$

The radial integration in Eq. (5) is performed first and results in a sum of two-dimensional integrals,

$$V_0\sum_{k=1}^{k'_p}d_k\int_0^\pi\int_0^{2\pi}[R(\theta,\phi)-R_{N_e}]^kY^*_{l,m}(\theta,\phi)\times Y_{l',m'}(\theta,\phi)\sin(\theta)d\theta\,d\phi\ , \tag{7}$$

where the coefficients d_k depend on the quantum number set $(n,\ l,\ n',\ l')$ and obviously on the size, and $k'_p=2k_p+3$. The spherical harmonics are factorized according to

$$Y_{l,m}(\theta,\phi)=C_{l,m}P_l^{|m|}[\cos(\theta)]e^{im\phi}\ , \tag{8}$$

where the functions $P_l^{|m|}$ are associated Legendre polynomials and the prefactors $C_{l,m}$ depend on l and m. The total matrix element is finally expressed as

$$V_0\sum_{k=1}^{k'_p}d_k\,A^k\alpha(l,m,l',m',n_1,k)\beta(m,m',n_2,k)+E_{n,l}\delta_{n,n'}\delta_{l,l'}\delta_{m,m'}\ , \tag{9}$$

with

$$\beta(m,m',n_2,k)=\int_0^{2\pi}\cos[(m'-m)\phi]\cos^k(n_2\phi)d\phi\ , \tag{10}$$

$$\alpha(l,m,l',m',n_1,k)=C_{l,m}C_{l',m'}\int_0^\pi P_l^{|m|}[\cos(\theta)]P_{l'}^{|m'|}[\cos(\theta)]\cos^k(n_1\theta)\times\sin(\theta)d\theta\ . \tag{11}$$

Expanding $\cos^k(n_2\phi)$ according to

$$\cos^k(n_2\phi)=\sum_{k'=0}^{k}c_{k',k}\cos(k'n_2\phi)\ , \tag{12}$$

[with k' odd (even) if k is odd (even)] allows us to write $\beta(m,m',n_2,k)$ as

$$\beta(m,m',n_2,k)=\frac{1}{2}\sum_{k'=0}^{k}c_{k',k}\int_0^{2\pi}\{\cos[(m'-m+k'n_2)\phi]+\cos[(m'-m-k'n_2)\phi]\}d\phi\ . \tag{13}$$

Analytical evaluation of β is straightforward, and the following selection rules for β result:

$$m'-m=-kn_2,-(k-2)n_2,\ldots,(k-2)n_2,kn_2\ . \tag{14}$$

The coefficients $\alpha(l,m,l',m',n_1,k)$ are evaluated numerically, except in the cases where direct application of the symmetry properties related to the inversion ($\pi-\theta\leftarrow\theta$) or of the orthogonality of the associated Legendre polynomials ($|m|$ fixed), leads to zero or a simple analytical result.

Because the length of the calculations increases drastically with the matrix size, identifying independent submatrixes to be diagonalized is highly advised. By taking into account the selection rules Eq. (14), it is obvious from Eqs. (9) and (14) that the large matrix $[M]$ associated with the whole truncated basis splits into N independent submatrixes, with $N=\min(n_2,2l_{\max}+1)$, where $l_{\max}$ is the highest angular momentum involved in the truncat-

ed basis. Each of these smaller matrixes $[M]_{m0}$ is characterized by the specific m values of their related subspace $\{m_0, m_0-n_2, m_0-2n_2, m_0-3n_2, \ldots\}$, where m_0 runs from $m_0=l_{\max}$ to $m_0=l_{\max}-(N-1)$. Each eigenvalue has a twofold degeneracy (spin degeneracy). Further reduction of the computational time is achieved owing to the symmetry properties of the roughness parametrization. Actually, for $n_2>2$, apart from the matrixes involving states with $m=0$ and, if n_2 is even, $m=n_2/2$, to each submatrix corresponds a distinct submatrix involving the negative of the m values characterizing the first one. These two submatrixes have the same eigenvalues, since they are merely related through the diagonal unitary transformation corresponding to a change of the conventional phase defining the spherical harmonics,

$$\langle \psi_{n,l,-m}|H|\psi_{n',l',-m'}\rangle = (-1)^{m+m'}\langle \psi_{n,l,m}|H|\psi_{n',l',m'}\rangle \ . \quad (15)$$

This additional degeneracy stems from the symmetry of the parametrization Eq. (1), with respect to the transformation $-\phi\leftarrow\phi$ (symmetry σ_v). Therefore, the levels of the Hamiltonian H have a fourfold, or a twofold (for the two specific above-mentioned cases), degeneracy.

III. RESULTS

A. Preliminary

The Wigner-Seitz radius corresponding to gallium metal ($r_s=2.191$ a.u.) is used in all the model calculations reported in this paper. However, we emphasize that we are only interested in the qualitative effects and trends related to the surface roughness, and that our results are quite general. The quantitative results we obtained are not directly applicable to the real gallium clusters, all the more that the "unperturbed" hard-walled potential well is a very crude zeroth-order approximation for the spherical effective electronic potential obtained in self-consistent KS calculations. Trends to be expected for other values of the valence number Z_v and Wigner-Seitz radius r_s will be briefly discussed in the conclusion Sec. IV.

The well depth is fixed to the value $V_0=-0.6$ a.u., leading to a bulk Fermi level in the "unperturbed" potential equal to $E_f\approx-0.22$ a.u. This depth value, lower than the mean depth obtained in local-density KS calculations ($V_0\approx-0.5$ a.u.), is chosen in order to slightly lower the effects due to the discretized continuum, where the energy spectrum is more congested. This reduces noticeably the number of positive-energy levels to be retained in the truncated basis. The influence of the location of the Fermi level relative to the vacuum level will be discussed.

The continuum is quantified by using the following parameters for the outer potential well: $\Delta=6$ a.u. and $V_1=0.4$ a.u. With these values, a sufficient convergence is obtained. For instance, with the parameter sets ($\Delta=9$ a.u., $V_1=0.4$ a.u.) and ($\Delta=6$ a.u., $V_1=0.6$ a.u.), the relative discrepancy $\delta E/E$ between the bound levels obtained with the three parameter sets is typically on the order of $10^{-6}-10^{-4}$ at the bottom of the inner well, and $10^{-4}-10^{-3}$ in the neighborhood of the Fermi energy. The degree of the polynomials fitting the radial functions [Eq. (6)] is fixed to the value $k_p=6$ for $A<3$ a.u. and $k_p=8$ for $A>3$ a.u. We would like to point out that the selected values for V_1, Δ, and k_p are largely overestimated for studying, through electronic DOS calculations, the qualitative effects arising from the surface roughness (the basis and matrix sizes are indeed very large). However, because the shell-correction energy is a very small fraction of the total electronic energy for large cluster sizes, very accurate eigenvalues are required in Secs. III B 3 and III C 2 to avoid spurious "shell" effects. Moreover, an enlarged basis ensures that the size discontinuities in the level-repulsion effects occurring when a new bound level is included in the truncated basis, are completely rubbed out for the low-lying states relevant to the electronic ground state of the cluster.

In Table I are listed, for different cluster sizes, data which are useful for analyzing the results. The largest angular momentum l involved in the ground state of the "unperturbed" Hamiltonian H_0' is indicated in column b. Except for large corrugation amplitudes A, and if one disregards the close vicinity of the Fermi energy, the N_e lowest states in the corrugated and unperturbed wells span essentially the same subspace. The highest angular momentum l in the truncated basis ($E_{n,l}<V_1$) is given in

TABLE I. Useful data for analyzing the results of Sec. III. Column a: the number of valence electrons N_e. Column b: the highest angular momentum l involved in the ground state for the "unperturbed" spherical potential well. Column c: the highest angular momentum involved in the truncated basis ($E_{n,l}<V_1$). Column d: the typical roughness parameter $n_{\rm cor}$ [n_i in Eq. (1)] corresponding to the unavoidable surface roughness related to the intrinsic granularity of the ionic background, for trivalent metals (see Sec. III A).

a N_e	b $l_{\max}$ (ground state)	c $l_{\max}$ (truncated basis)	d $n_{\rm cor}$
100	5	11	9
200	8	14	11
300	9	16	13
400	10	18	14
500	11	20	15
600	12	21	16
700	13	22	17
800	13	23	18
900	14	25	19
1000	14	26	19
1100	15	26	20
1200	15	27	21
1300	16	28	21
1400	16	29	22
1500	17	30	22
1600	17	30	23
1700	18	31	23
1800	18	32	24
1900	19	32	24
2000	19	33	25

column c. The n_{cor} values in column d correspond to the typical wavelength associated with the unavoidable surface corrugation related to the background granularity, and consistent with the square surface lattices of bumbs and hollows in the equatorial region. The order of magnitude of n_{cor} is easily deduced as follows. Considering that to each ion corresponds a cubic cell of volume a^3 defined by $a^3=4\pi r_s^3 Z_v/3$, the typical n_{cor} value is estimated by equating a with the spatial period d_{cor} of the square lattice of bumps. One obtains $d_{cor}=2^{-1/2}(2\pi R_{N_e}/n_{cor})=1.6Z_v^{1/3}r_s=0.7\lambda_f$ and $n_{cor}=2.8(N_e/Z_v)^{1/3}=1.94N_e^{1/3}$. Since the wavelength of the roughness decreases along the ϕ coordinate at the polar regions, the effective "grain" of the corrugation, averaged over the whole surface, is however slightly finer. We remark that the roughness grain linked to the intrinsic granularity in actual clusters is expected to depend on the surface structure, as in faceted polyhedral clusters. So the above value has only to be considered as a rough estimation. In Sec. III B, we have assumed n_{cor} values slightly larger than those indicated in Table I in order to provide a complete investigation of the roughness effects as a function of the model parameter n_{cor} (up to $n_{cor}=30$). The results are nevertheless interesting and useful. If a non-sine-wave periodic corrugation is assumed, the expansion of $R(\theta,\phi)$ into a Fourier series in Eq. (7) may involve non-negligible harmonic terms with very large n_{cor} values. The calculations reported in Sec. III B are thus not at all academic.

With regard to the total height of the bumbs on the surface of the electronic potential ($2A$), only a rough estimation can be given. As for the n_{cor} parameter, the typical height depends on the ionic structure—liquidlike or layering—over the surface. In addition, because kinetic effects prevent the electronic cloud from responding to sharp spatial changes of the background pseudopotential or structure,[43] the roughness amplitude of the total KS-electronic potential cannot be quantitatively inferred, in a simple way, from background parameters, such as the effective ion core-radius and the average ion-ion distance. In the case of gallium (Ga^{3+} ionic radius ≈ 1.17 a.u., average ion-ion distance on the order of 5–6 a.u.), we think that values up to $2A=3$–4 a.u. are reasonably consistent with a liquidlike surface structure.

B. Effects of short-wavelength roughness

1. *Is a rough potential equivalent to a soft one?*

Does a rough electronic potential generate the same electronic shell structure as a soft potential having a perfect spherical symmetry? Or in other words, is a rough step-walled jellium equivalent to a soft one? In a previous work,[16] a positive answer was assumed for explaining partly the large shift of the supershell node (as compared to the JM prediction) observed in mass spectra of trivalent metals.[6,30] This assumption has been formulated more precisely in Ref. 19 by stating that, provided that an average homogeneity and an overall spherical shape are ensured, the size evolution in the electronic cluster properties can be reliably calculated in keeping only the spherical component $V_{sph}(r)$ of the KS-electronic potential $V(\mathbf{r})=V_{sph}(r)+V_{ang}(r,\theta,\phi)$, or in practical calculations in spherically averaging the total ionic pseudopotential prior to KS calculations. Support for this assumption is provided by the following crude first-order perturbative analysis. Let us consider the subspace corresponding to a single degenerate level $E_{n,l}$, eigenvalue obtained in retaining only the component $V_{sph}(r)$ in the Schrödinger equation. At the lowest order of the perturbation theory, the effect of $V_{ang}(\mathbf{r})$ consists only in a level splitting (new orbital eigenstates Ψ_i), with a shift of the average energy,

$$\Delta E_{n,l}=2\sum_i \langle \psi_i | V_{ang} | \psi_i \rangle = \int \rho(r) V_{ang}(\mathbf{r}) d\mathbf{r} , \qquad (16)$$

equal to zero since the electron density $\rho(r)$ associated with a filled $2(2l+1)$-fold degenerate level $E_{n,l}$ is only r dependent and the spherical average of $V_{ang}(\mathbf{r})$ is by definition equal to zero. The same analysis applies to the larger subspace associated with a level bunch. Since the shell effects and the magic sizes are determined by the ordering and degeneracy of the levels and bunches, the "level broadening" induced by $V_{ang}(\mathbf{r})$ is expected to give rise to a weakening of the shell effects only. Our nonperturbative calculations confirm this crude qualitative analysis.

2. *DOS calculations*

Electronic DOS curves corresponding to the size $N_e=801$, for increasing roughness amplitude A, are plotted in Fig. 3, and compared to the DOS obtained with the unperturbed potential well [Fig. 3(a)]. The grain of the roughness ($n_{cor}=25$) is finer than the one related to the intrinsic discreteness of the ionic frame (see Sec. III A and Table I). Two main results emerge clearly from this figure.

(i) The level broadening is almost nonexistent along the entire bound spectrum, and is noticeable only in the upper region of the DOS just below the vacuum level $E=0$. More precisely, the effective broadening is smaller than the full width at half maximum (FWHM) of the Lorentzian curve (0.0025 a.u.) taken for convoluting the discrete DOS. In Fig. 3, the level splittings are essentially reflected through the lowering of the peak height and an increase of the DOS minima. Let us emphasize that the height increase of some peaks, as compared to their height in Fig. 3(a), results from both a tiny change in the level bunching and the convolution with a finite-width Lorentzian curve (several close levels, each of them undergoing a specific shift, underlie most of the peaks displayed in Fig. 3).

(ii) The energy levels $E_{n,l}$ move up. The shift becomes larger as the roughness amplitude and the energy increase, and moreover a slight l dependence is observed: levels of high angular momenta l (the highest peaks, in general) are more strongly pushed up than those of lower l values (the smallest peaks in general). The correlation (increasing shift versus the peak height) apparently fails for some displayed peaks, particularly in the upper ener-

gy domain ($E \approx 0$), where the discrete DOS are more congested. Origin of the apparent failure was already pointed out: the peaks are in fact bunches of very close levels and the peak height is often related to the sum of all the level degeneracies. Inspection of the discrete DOS confirms this analysis. A change in the level-bunching results from the l dependence of the level shift. In particular, the supershell beat, characterized by a frequency doubling in the DOS pattern, has been shifted up by the roughness effects. The nodal structure is not easily discernible at first glance in Fig. 3, because the FWHM of the convoluting Lorentzian profile is small. By contrast the overall supershell structure emerges clearly when the FWHM is increased. The node patterns, indicated in Fig. 3 by short horizontal lines, have been located by a prior smoothing of the sharp DOS curves. For a large enough roughness amplitude, it is obvious that there is no beat in the DOS curve below $E=0$ [Fig. 3(d)].

The two above features can be more quantitatively grounded from mathematical inspection of the matrix elements of the perturbation. With regard to the removal of the $(2l+1)$-fold orbital degeneracy of the level $E_{n,l}$, the strict and approximate selection rules for the coefficients β [Eq. (14)] and α [Eq. (11)] give rise to weak or large level splittings, depending on the n_i and l values.

If $n_2 > 2l$, the only nonzero matrix elements within the $E_{n,l}$ subspace are necessarily the diagonal ones [Eqs. (13) and (14) imply $k'=0$, and then $m'=m$]. Only the even values of k in Eqs. (9) ($k=2,4,\ldots$) contribute to the matrix element, and from Eq. (13) one obtains $\beta = 2\pi c_{0,k}$. From the expansion of $\cos^k(n_1\theta)$, according to Eq. (12), it is clear that, since $\cos(k' n_1 \theta)$ is—for $k'=2,4,6\ldots$—a rapidly oscillating function with a zero average, that the major contribution in the integral Eq. (11) is brought by the term $k'=0$, particularly as $|m|$ becomes larger. We recall that $P_l^{|m|}$ is the product of $|\sin(\theta)|^{|m|}$, by a polynomial of degree $(l-|m|)$ in $\cos(\theta)$. From the orthogonality property of the associated Legendre polynomial,

$$\int_0^{\pi} P_l^{|m|}[\cos(\theta)] P_{l'}^{|m|}[\cos(\theta)] \sin(\theta) d\theta = \frac{\delta_{l,l'}}{2\pi [C_{l,m}]^2} , \tag{17}$$

we finally obtain, within the $E_{n,l}$ subspace, a scalar submatrix

$$\left\{ V_0 \sum_{k=2,4,\ldots,}^{k_p'} d_k A^k (c_{0,k})^2 + E_{n,l} \right\} \delta_{m,m'} . \tag{18}$$

The same analysis holds true when n_2 is smaller, but not too much, relative to $2l$. In this case, Zeeman states such as $|m'-m| = n_2$ can be coupled [$k'=1$ or -1 in Eq. (14)] via the odd values of k in Eq. (9) ($\beta \neq 0$). However, since $|m|$ and $|m'|$ are necessarily close to l ($n_2 \lesssim 2l$), the product of the two Legendre polynomials in Eq. (11) has a slow behavior as a function of θ, as compared to the rapid oscillations of $\cos^k(n_1\theta)$, and, therefore, the integral α will be close to zero. The $E_{n,l}$-submatrix is then approximately the same as previously.

If $n_2 \ll 2l$, the above analysis does not apply. The submatrix contains nonzero off-diagonal matrix elements and m-dependent diagonal ones. Consequently, a noticeable level splitting occurs simultaneously with the global shift. For the bound spectrum $E<0$, in particular, the whole domain below the Fermi energy, conditions $n_2 > 2l$ or $n_2 \lesssim 2l$ are fulfilled and only the level shift prevails. In the upper energy domain, where higher l values are involved, the level-broadening effect becomes more apparent.

In the previous analysis, the interaction between distinct levels $E_{n,l}$ and $E_{n',l'}$ have been ignored. If one disregards the highest angular momenta involved in the truncated basis, which are energetically far above the Fermi level (these levels are close to V_1), the condition $n_2 > (l+l')$ or $n_2 \lesssim (l+l')$ is approximately fulfilled and the same analysis can be carried out. Considering that the largest matrix elements are those with $m=m'$, and using Eq. (17), one finds finally that, in the first approximation (i) levels having different angular momenta interact only weakly and, (ii) the repelling effects between the levels having the same l value occur without appreciable level splitting (poor m dependence of the matrix elements).

Explicit support for the spherical averaging approximation is derived in assuming the strict applicability of the numerical selection rules for the coefficients β and α within the whole basis space. This is achieved formally

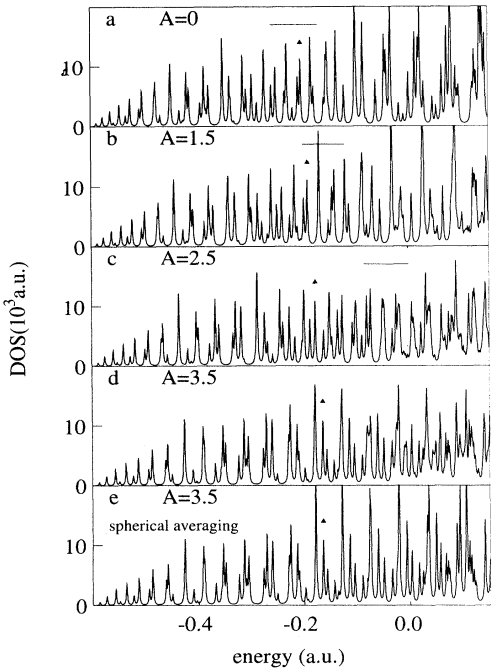

FIG. 3. Electronic DOS curves corresponding to the size $N_e=801$, for various radial roughness amplitudes A (in atomic units) and $n_{\rm cor}=n_1=n_2=25$ in Eq. (1). The DOS have been convoluted with a Lorentzian-shaped profile having a FWHM equal to 0.0025 a.u. The Fermi energy is indicated by a triangle. The short horizontal line indicates the location of the supershell beat pattern. This location has been determined by further smoothing the DOS curves.

by taking the limit $n_{\rm cor}\rightarrow\infty$ in the mathematical expressions. One obtains the total matrix element,

$$\left\{V_0\sum_{k=2,4,\ldots,}^{k_p'} d_k A^k (c_{0,k})^2+E_{n,l}\delta_{n,n'}\right\}\delta_{l,l'}\delta_{m,m'} . \quad (19)$$

Since $(c_{0,k})^2$ is the spherical average of $\cos^k(n_1\theta)\cos^k(n_2\theta)$, Eq. (19) is manifestly, in view of Eq. (7), the Schrödinger equation—in matrix form—involving the $V_{\rm sph}(r)$ component only. The matrix element Eq. (19) will be referred to as "the spherical averaging approximation" in the following. This approximation leads to the same electronic DOS as previously, over the whole energy domain relevant to the ground state [compare Figs. 3(d) and 3(e)].

These calculations corroborate the surmise stating that the electronic shell structure is governed, for the most part, by the spherical average of the effective potential, provided that approximate spherical shape and background homogeneity are ensured. A $n_{\rm cor}$ value larger than the one given in Table I has been assumed, but we would like to emphasize that identical conclusions would be drawn in using the specific value corresponding to the intrinsic granularity, except for a slight increase of the level-splitting effects. Moreover, these results demonstrate that, in the case of a fine surface-roughness grain, the effective level broadening is negligible, even in the case of a large roughness amplitude along the radial coordinate. A short-wavelength corrugation is thus expected to have a minor influence on the magnitude of the shell effects in mass spectra.

3. *Shell-correction energy calculations*

We now attempt to estimate accurately the size shift of the supershell node. Qualitative information about the node location can be gained from DOS curves as those displayed in Fig. 3, by comparing the location of the frequency-doubled pattern relative to the Fermi energy. However, except for infinite-depth hard-walled spherical potential wells in which the levels scale perfectly as R^{-2} as a function of the well radius, a size-dependent reorganization of the level bunches occurs simultaneously with the packing down of the electronic spectrum when soft potential walls are involved.[44] In consequence, reliable determination of the beat location and magic sizes requires us to perform calculations for numerous sizes. For this purpose, and in order to illustrate the poor weakening of the shell effects too, we have calculated for each cluster size ($\Delta N_e=3$, 6, 9 in the size ranges [3–1000], [1000–1500], [1500–2000], respectively), the electronic energy $E(N_e)$ of the ground state and the Fermi level $E_f(N_e)$. $E(N_e)$ is taken as the sum of the energies of the N_e lowest bound states, as it was usually assumed in the independent-electron approximation. The overall shell and supershell structures can be made visible to the eye by plotting the shell-correction energy or the ionization potential (IP) as a function of the cluster size. For the IP, we have used the approximate formula derived from the Koopmans' theorem by Brack, Genzken, and Hansen[45]

$$\mathrm{IP}(N_e)=-E_f(N_e)+\frac{1}{2R_{N_e}} . \quad (20)$$

The shell-correction energy is obtained by substracting from $E(N_e)$ the smooth part, i.e., the contribution that varies smoothly with the particle number.

The roughness parameters $n_{\rm cor}$ and A have been kept constant over the whole size domain. Apart from the observation that our simple parametrization Eq. (1) is unsuitable to properly model the size-to-size evolution of the surface roughness of real clusters, this constraint is dictated by the fact that the shell-correction energy is a very small part of the total electronic energy $E(N_e)$, and thus any size discontinuity in the selected model parameters would blur the shell effects. Obviously this rather unphysical prescription has to be kept in mind when the results are analyzed.

The second point we want to emphasize concerns the approximate method used to extract the shell-correction energy from $E(N_e)$. When smoothly shaped potentials are involved, refined methods for determining the average part of $E(N_e)$, such as the Strutinsky's averaging technique in nuclear physics,[46] are available. In practice, guiding by the liquid-drop-model (LDM) picture applied to a structureless cluster, the smooth part can be accurately parametrized by the best third order in $N_e^{1/3}$ polynomial fit of $E(N_e)$, provided the size domain is large enough to include numerous shell size periods. This smooth part accounts for the so-called volume, surface, and curvature energies. It is tempting to determine the whole effects arising from both the electronic shell and surface corrugation effects by imposing the LDM volume, surface, and curvature coefficients obtained with the "unperturbed" spherical potential well $V'(r)$ Eq. (3). However, in applying this procedure, one obtains a large shell plus corrugation energy, which does not display clearly the electronic shell effects under investigation: the electronic shell-related modulations are superimposed on a size-dependent background of large magnitude. The same feature is also observed—however to a much lesser extent—when the constraint on the expansion coefficients is relaxed and the smooth part of $E(N_e)$ is derived by performing the usual best third-order polynomial fit, especially when large A and low $n_{\rm cor}$ parameters are assumed. Actually, this large residual background, originating from the effects of the surface roughness on the level spectrum, is due to the fact that, when highly distorted potential walls are involved, the volume, surface, and mean curvature of the potential well do not scale as N_e, $N_e^{2/3}$, and $N_e^{1/3}$, respectively (especially for small sizes), unlike a perfect sphere. For instance, the roughness parametrization Eq. (1) leads to expansions of the form

$$N_e^s\left\{\sum_{j=0}^{j_{\max}} a_j(n_{\rm cor})\left[\frac{A}{R_{N_e}}\right]^j\right\} , \quad (21)$$

where $s=1,\frac{2}{3}$ and $j_{\max}=2,\infty$ for the volume and the surface, respectively. Let us remark that the $n_{\rm cor}$-dependent coefficients a_j may be large when the roughness wavelength decreases. In fact, when A or/and $n_{\rm cor}$ are large,

the usual LDM expansion is an unsuitable concept for parametrizing the smooth part of $E(N_e)$. For instance, when $n_{cor} \to \infty$ the surface of the corrugated well becomes infinite and the LDM expansion manifestly fails. From a quantum-mechanical point of view, it is clear that spatial details having short wavelengths relative to the electronic de Broglie ones are immaterial. Therefore, the *effective* volume and surface explored by the electron do not coincide necessarily with the geometrical counterparts. When the roughness amplitude A increases, our calculations indicate that the *effective* volume probed by the electrons decreases (this is the main origin of the A dependent shift of the Fermi level in Fig. 3), unlike the geometrical volume enclosed by $R(\theta,\phi)$. Owing to these difficulties, we have followed the pragmatic procedure consisting in increasing progressively the order of the $E(N_e)$-polynomial fit until the shell-correction energy oscillates around the value zero. For a small roughness amplitude A, the usual third-order polynomial parametrization of $E(N_e)$ is sufficient. In any case up to two additional terms at the maximum, according to the expansion Eq. (21), were added to prevent eventual spurious effects from altering the shell-related oscillations.

Results are displayed in Figs. 4 and 5. The shell-energy curves exhibit clearly the usual shell and supershell patterns related to the spherical symmetry, characterized by a shell size spacing equal to $\Delta N_e^{1/3} \approx 0.6$ and a half-period shift of the major shell closing numbers (the sharp dips in the displayed curves) in the nodal region. Specific effects arising from the surface roughness are deduced immediately by comparing these curves with the electronic structure in the "unperturbed" potential well

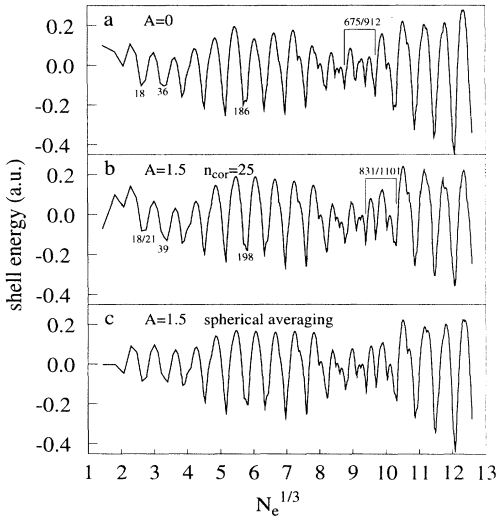

FIG. 4. The shell-correction energy as a function of the cluster size. Some low magic numbers are indicated (step $\Delta N_e = 3$ in the size range $3 < N_e < 1000$). The extent of the supershell beat pattern is roughly characterized by the highest (lowest) clear magic size spaced from the previous (following) ones by the shell size period $\Delta N_e \approx 0.6$. (a) No surface roughness. (b) $A = 1.5$ a.u. and $n_i = 25$ in Eq. (1). (c) Result of the spherical averaging approximation Eq. (19) for $A = 1.5$ a.u.

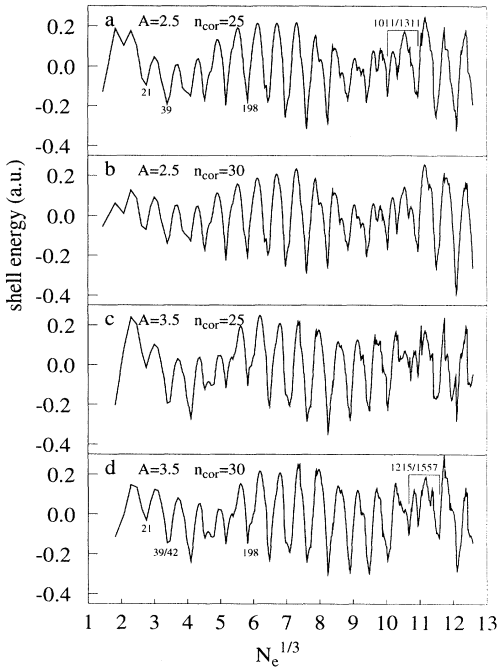

FIG. 5. Same as the caption of Fig. 4, except for the roughness parameters A and $n_{cor} = n_1 = n_2$, which are indicated above the curves.

$V'(r)$[$A = 0$, Fig. 4(a)]. In a first approximation, whatever the radial corrugation amplitude A is, the differences are the same as those signing a softness increase of the surface-potential profile, namely, a slight (large) shift of the magic sizes (beat pattern) towards larger sizes.[16] Exact locations of the supershell nodes are not easy to determine, because the subshell-related structures often obscure the pattern in this size domain and the decrease of the shell effects is rather weak. Nevertheless the extent of the beat size domain has been roughly characterized by the highest (lowest) clear magic size spaced from the previous (following) ones by the shell period $\Delta N_e^{1/3} \approx 0.6$. In any case, the supershell node shift is unquestionable, and is found directly correlated to the radial amplitude of the corrugation. One can notice the poor dependence of the overall shell and supershell structures on the n_{cor} parameter. Actually the n_{cor} values involved in the present calculations are large and the electronic structure is essentially ruled by the spherical averaging approximation Eq. (19), especially for small roughness amplitudes A [compare Figs. 4(b) and 4(c)]. From a simple glance at the roughness parametrization Eq. (1) it is rather intuitive that the effective softness of the rough surface (i.e., the surface profile of the spherically averaged potential well) is weakly dependent on the parameter n_{cor} and on the size (see below). Increasing the n_{cor} parameter beyond the value $n_{cor} = 25$ leads to results almost identical to those obtained in assuming strictly the spherical averaging approximation Eq. (19).

When the parameter A (n_{cor}) increases (decreases), the failure of the spherical averaging approximation becomes more and more apparent in the upper size range. The

effects of the level broadening and mixing are stronger, and lead to a noticeable weakening of the shell oscillations and eventually to a large change in the state bunching. Let us emphasize that some of the *smallest* "noisy" structures observed in Fig. 5 might be due to eventual numerical rounding errors, owing to the large sizes of the matrixes to be diagonalized. However, since the formal structure of the matrixes does not depend on A, the largest sharp structures observed in Fig. 5 (compare with Fig. 4) are not computational artifacts, but undoubtedly reflect large reorganizations in the state distribution. In the upper size range, the length scales of the surface bumps and hollows along the angular coordinates are comparable to the Fermi wavelength. Hence the roughness begins to be effectively felt by the electrons, and the specific level bunching in the rough potential may develop, all the easier the larger the size. If one disregards the shell-correction energy in Fig. 5(c), which corresponds to an amplitude A inconsistent with a liquidlike surface structure, the strength of the shell effects is only very slightly weakened along the entire size range displayed ($N_e=3-2000$) for $n_{\rm cor}=25$. Since this value is the one associated with the minimal grain for the size $N_e=2000$ (see Table I), we can reasonably conclude that the electronic shell structure is governed by the spherical averaging approximation Eq. (19) for each cluster size when the grain of the surface roughness is minimal. Calculations of electronic DOS at several sizes confirm this statement. An immediate support is provided by the data in Table I, in noting that the ratio $n_{\rm cor}/2l_{\rm max}$ (ground state) is almost constant (0.6–0.7), with a slightly increasing trend when the size decreases. Hence the analysis reported in Sec. III B 2, which grounds the spherical averaging approximation, applies for each cluster size. Actually this result is a consequence of the quasi-size independence of the ratio between the Fermi-wavelength and the average ion-ion distance, which imposes the grain of minimal roughness.

The spherical component $V_{\rm sph}(r)$ of the rough inner potential well $V(\mathbf{r})$,

$$V_{\rm sph}(r)=\frac{V_0}{4\pi}\int_0^{\pi}\int_0^{2\pi}\Theta[R(\theta,\phi)-r]\sin(\theta)d\theta\,d\phi\ , \qquad (22)$$

is plotted in Fig. 6 for the radial corrugation amplitudes $A=1.5$, 2.5, and 3.5 a.u. As expected, the softness of the surface profile increases with increasing amplitude A. From Eq. (1), $V_{\rm sph}(r-R_{N_e})$ is manifestly independent of R_{N_e}, and we have numerically checked that this independence holds true in respect of the parameter $n_{\rm cor}$. The surface thickness is only partially probed by the electrons. The upper radial bound is roughly located at the outer turning point of the classical oscillation along the diameter, at the Fermi level ($E_f\approx -0.2$ a.u., see Fig. 3). In fact, this outermost radial domain is relevant only for the highest occupied quantum levels of low angular momenta. As discussed previously, the volume of the potential well, which is effectively explored by the electrons, is smaller than the one enclosed by the corrugated surface, since the radial extent of most of the occupied levels are located below $r=R_{N_e}$. Figure 6 clearly suggests that, for a given corrugation parameter set ($A,n_{\rm cor}$), the effective surface softness, and in consequence the electronic shell and supershell patterns, depend on the location of the Fermi level relative to the vacuum level, or in other words on the potential depth $|V_0|$. This feature has been confirmed by calculating shell-correction energy curves for lower potential depth $|V_0|$. In order to preserve a high accuracy in the computation of the eigenvalues, the parameter V_1 of the outer potential well has been enlarged ($V_1=0.5$ a.u.), ensuring, therefore, a correct overall level repulsion from the upper part of the electronic spectrum. As expected, the supershell node was found slightly shifted towards larger sizes relative to the beat location obtained with $V_0=-0.6$ a.u. For instance, with the parameter set ($A=3.5$ a.u., $V_0=-0.45$ a.u.), the supershell node is enclosed by the magic sizes 1455 and 1827 [compare with curve 5(d)].

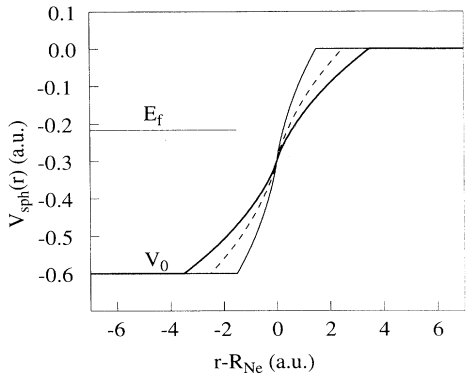

FIG. 6. The spherical average $V_{\rm sph}(r)$ of the corrugated potential [Eq. (22)], for the radial roughness amplitudes $A=1.5$ (thin line), 2.5 (dashed line), and 3.5 a.u. (thick line). The rough surface is parametrized according to Eq. (1). The soft surface profile does not depend on R_{N_e} and $n_{\rm cor}$. The horizontal line indicates the location of the Fermi energy in the bulk limit.

From the semiclassical approach, the $N_e^{1/3}$ scale is known to be more appropriate to quantify the intrinsic impact of the surface potential shape on the size dependence of the electronic shell structure. Figures 4 and 5 show that a quite reasonable corrugation is likely to induce a supershell node shift on the order of $\Delta N_e^{1/3}=1$. This shift is far from being negligible on the N_e scale, especially if a large number of electrons is involved. The shift on the N_e scale may be spectacular but, experimentally, is not necessarily easy to detect in mass spectra, because it involves one or two fringes at the maximum, in a size domain where the signal modulations are weakly contrasted and often blurred. A quantitative estimation of the roughness effects on real clusters is hazardous, because the actual corrugation is unknown, and undoubtedly depend on the experimental conditions prevailing during the cluster growth. Moreover, it is not definite that the net beat shift, arising from both the surface lattice corrugation and the pseudopotential effects, can be estimated by adding the two respective individually estimated contributions.

C. Effects of long-wavelength roughness

1. DOS calculations

DOS curves corresponding to the size $N_e=801$ and $A=1.5$ a.u., for decreasing n_{cor}-values, are plotted in Fig. 7. As in Fig. 3, the discrete DOS have been convoluted with a Lorentzian curve having a FWHM equal to 0.0025 a.u. For $n_{cor}=20$ (a value close to the n_{cor} value of minimal grain, see Table I), no DOS change below the Fermi level is observed, as compared to the results obtained with larger n_{cor} parameters [$n_{cor}=25$, see Fig. 3(b)]. Above the Fermi energy the level bunching remains strong. However, the level broadening and mixing effects are noticeable and are reflected through a regular increase of the minima between the shells as a function of the energy E. When n_{cor} decreases, i.e., when the surface-roughness wavelength increases, both effects are magnified and extend more and more deeply below the Fermi level. A contrasted electronic shell structure is preserved in the lowest part of the potential well only. Roughly, this energy domain involves angular momenta such as $2l \lesssim n_{cor}$. For small enough values of n_{cor} (the range depends obviously on the parameter A), the standard electronic shell structure is completely destroyed in the neighborhood of the Fermi level, owing to the strong level mixing. One can note that the decrease of the n_{cor} parameter below a particular threshold value does not modify qualitatively the overall spectrum in this region (with respect to the entire spectrum, the only noticeable change is the spreading of the roughness effects towards the bottom of the potential), indicating that the extent of the level or bunch splittings has reached a magnitude comparable to the initial energy gaps. The remaining "noisy" structures of various scales in the electronic DOS are due to the reminescence of the overall spherical symmetry and to the finite size of the system (statistical fluctuations).

However, let us emphasize that, in enlarging still more the angular wavelength of the corrugation, simplification of the spectrum is expected to occur. Actually, in such cases, speaking of shape-deformation effects instead of roughness effects would be more appropriate. The reason is that, for very low n_{cor} values, the picture of a "perturbed" sphere, implying the smoothing of the shell structure through the removal of the orbital degeneracy, is no longer suitable: the level-bunching scales associated with the specific classical orbits available in the deformed wells are expected to prevail more and more, because the spatial extent of the bumps and hollows exceeds considerably the de Broglie wavelengths of the wave functions. For the reader's information, let us note that the mathematical framework of Sec. II can be used to calculate electronic DOS for prolate or oblate cluster shapes, by taking the parameter sets ($n_1=2$, $n_2=0$, $A>0$) and ($n_1=2$, $n_2=0$, $A<0$), respectively, in the roughness parametrization Eq. (1).

Similar DOS curves have been calculated for larger roughness amplitudes A. Qualitatively, the DOS curves are similar to those displayed in Fig. 7, but, quantitatively, the level-splitting and -mixing effects are much more pronounced for intermediate n_{cor} values.

2. Shell-correction energy and ionization-potential calculations

In order to investigate the size dependence of the survival of the electronic shell structure at the Fermi level, we have calculated the shell-correction energy ($A=1.5$ a.u., Fig. 8) and IP ($A=2.5$ a.u., Fig. 9) curves corre-

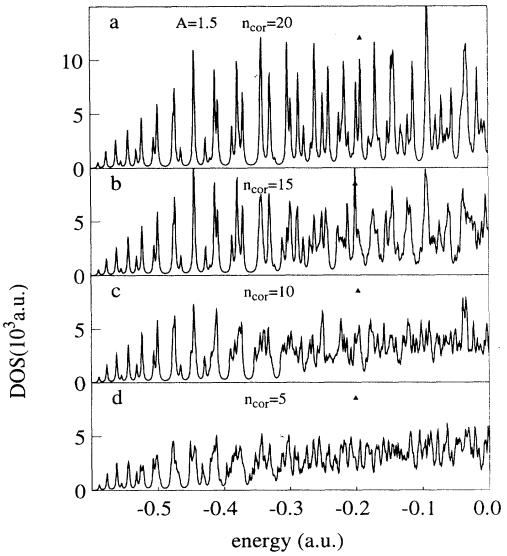

FIG. 7. Electronic DOS curves corresponding to the size $N_e=801$, for a decreasing value of the roughness parameter $n_{cor}=n_1=n_2$ in Eq. (1). The radial roughness amplitude A is equal to 1.5 a.u. The discrete DOS have been convoluted with a Lorentzian-shaped profile having a FWHM equal to 0.0025 a.u. The Fermi energy is located by a black triangle.

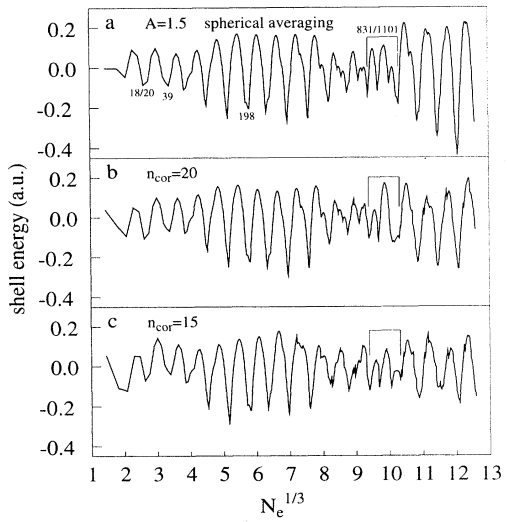

FIG. 8. Shell-correction energy as a function of the cluster size, for low values of the roughness parameter $n_{cor}=n_1=n_2$ in Eq. (1). The radial roughness amplitude is equal to 1.5 a.u. The extent of the supershell beat pattern is indicated by a short horizontal line. (a) Result of the spherical averaging approximation Eq. (19). (b) $n_{cor}=20$, (c) $n_{cor}=15$.

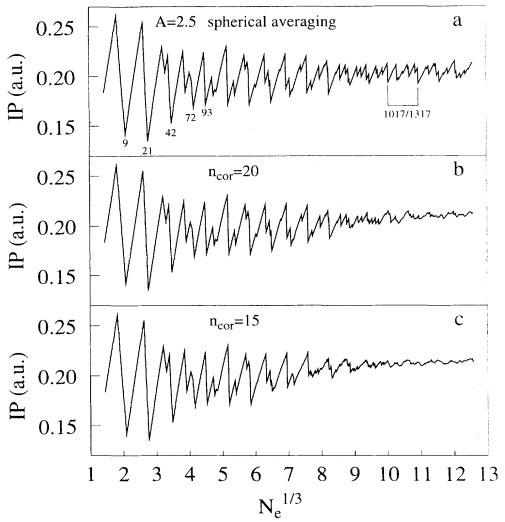

FIG. 9. Evolution of the ionization potential [Eq. (20)] as a function of the cluster size, for low values of the roughness parameter $n_{cor}=n_1=n_2$ in Eq. (1). The radial roughness amplitude is equal to 2.5 a.u. (a) Result of the spherical averaging approximation Eq. (19). The extent of the supershell beat pattern is indicated by a short horizontal line (b) $n_{cor}=20$. (c) $n_{cor}=15$.

sponding to the intermediate n_{cor} values 20 and 15. With lower values, the computational time becomes too prohibitive owing to the considerable increase of the matrix sizes. Results obtained with $A=3.5$ a.u. are qualitatively similar to those corresponding to the roughness amplitude $A=2.5$ a.u.

For $A=1.5$ a.u., the overall shell and supershell structures are similar to those obtained in the spherical averaging approximation [Fig. 8(a)]. The shell energy curve is practically unchanged as long as the Fermi wavelength remains noticeably larger than the surface-roughness wavelength along the angular coordinates, namely, if $2l$ is not too large as compared to n_{cor} for all the angular momenta l involved in the ground state. When the size increases, this condition is no longer fulfilled and the peak-to-peak amplitude of the shell modulations weakens appreciably, owing to the magnifying of the level broadening and mixing effects. However, the oscillations in the shell-energy curve remain strongly contrasted over the entire size range studied, as do the shell-related oscillations in the DOS curves in Fig. 7.

For a large amplitude A, the roughness effects increase considerably, in accordance with the calculated DOS curves. The decrease of the Fermi level as a function of the size, originating from the size dependence of the effective volume probed by the electrons [for a given n_{cor} parameter, the probing of the surface bumps, i.e., the geometrical volume enclosed by $R(\theta,\phi)$, is more effective when the size increases], counterbalancing thus the electrostatic contribution in Eq. (20), is responsible for the slight increasing trend of the IP curves in Fig. 9. This behavior has to be disregarded because it results from the constraint $n_{cor}=$const. The disappearance of the shell- and subshell-related sawtoothlike (characteristic of the independent-electron approximation) oscillations signs the onset of the washing out of the electronic shell structure at the Fermi level. However, it is worthwhile to note that some large-scale oscillations survive in spite of the considerable weakening. This indicates that the level bunching related to the spherical symmetry is not completely overcome by the roughness effects. The same holds true in respect of the shell-correction energy curves which, as compared to the IP curves, are less blurred by the subshell-related effects. In fact, when the average background is locally removed, the shell-correction energy curves look like the right part of curve c in Fig. 5, except for both a more pronounced weakening of the oscillations and a much more developed "noisy" structure. A trace of some oscillations related to the spherical symmetry are clearly identified but, in any case, the beat pattern is blurred and sometimes disappears.

IV. CONCLUSION

In this paper, we have studied the effects of surface roughness on the electronic shell and supershell structures of simple metal clusters. Unlike most of the previous published works, in which the tight-binding formalism is applied to bulklike cluster structures, our nonperturbative approach involves a finite-depth hard-walled spherical potential well with a sine-wave corrugation along the two angular coordinates. Our results may be summarized as follows, depending on the spatial periods of the surface corrugation relative to the Fermi wavelength λ_f.

(1) When the wavelengths of the surface roughness are comparable to or shorter than λ_f (the corrugation linked to the intrinsic granularity of the ionic frame fulfills this requirement), the electronic shell structure related to the spherical symmetry is preserved. The weakening of the shell effects, which is expected owing to the removal of the $(2l+1)$-fold orbital degeneracy, is minor, except for very large radial roughness amplitudes. The entire electronic shell structure is found to be ruled by the spherical average of the potential well. This result proves that a fine-grained hard-walled corrugated potential is, with regard to the electronic shell structure, equivalent to a spherically symmetric potential with a soft surface profile. In consequence, the magic sizes (supershell node locations) are slightly (noticeably) shifted towards higher sizes. Surface roughness is thus a possible candidate for explaining part of the supershell node shift observed in trivalent metal mass spectra.[6,30]

(2) When the wavelengths of the surface roughness along the angular coordinates are long, as compared to λ_f, the standard electronic shell structure is washed out, except for small radial corrugation amplitudes. However, apart from the supershell pattern, which seems completely wiped out, the reminescence of the level-bunching related to the overall spherical symmetry remains visible in spite of the considerable smoothing of the electronic DOS arising from the level-broadening and -mixing effects. Roughly the vanishing of the usual shell structure occurs when the radial and angular actions $p_f d_{cor}$ associated with the surface distortions exceed significantly the Planck constant (p_f is the Fermi

momentum and d_{cor} is the spatial extent of the bumps along the radial or angular coordinates). By invoking the semiclassical picture it is expected that, when this condition is satisfied, the specific classical trajectories—and consequently the related "level-bunching organization"—in the rough potential-well prevail: the nonspherical component of the surface roughness no longer acts as a weak perturbation on the highly degenerate spectrum obtained in retaining only the spherical component. This difference in physical effects, depending on the ratio d_{cor}/λ_f, has already been discussed by Lombardi *et al.* in the context of the classical chaos and its correspondence in quantum mechanics.[47]

Involving a nonsine-like periodic corrugation in Eq. (1) would not change qualitatively the above results. By expanding the surface boundary $R(\theta,\phi)$ into a Fourier series, it is quite intuitive that the fundamental term, having the longest spatial period, will govern the electronic shell structure, since the selection rules Eq. (14) corresponding to the harmonic terms reduce essentially to the simple condition $m'=m$ over the whole bound spectrum, except in the case of very large angular periods (very low n_{cor} values). In other words the effective surface softness of the rough potential will depend on the specific corrugation parametrization, but the magnitude of the level broadening and mixing effects will be mainly governed by the fundamental term of longest period, which implies the least drastic selection rules among the Zeeman m states.

In addition to the unavoidable roughness linked to the background granularity, actual cluster shapes may involve simultaneous distortions of various angular scales. The clear observation of the JM-like electronic shell structure up to very large sizes in Refs. 4, 6, and 30 suggests that the surface of liquidlike clusters is not dominated by static deformations or temperature-induced fluctuations having long wavelengths along the angular coordinates.

With regard to the level-splitting and -mixing effects arising from the unavoidable background granularity, the above conclusions are valid—all the more—in the case of alkali species, since the corresponding n_{cor}-value scales as $Z_v^{-1/3}$ (see Sec. III A) and the $E_{n,l}$-level set involved in the ground state is poorly dependent on the element. However, one can argue that the level spectrum is more congested and that consequently the level broadening and mixing effects will be much more pronounced (the level gaps scale roughly as r_s^{-2}). However, seeing that the matrix elements of the perturbation are proportional to V_0 (for instance, the potential bottom V_0 is on the order of -0.2 a.u. and -0.3 a.u. for sodium and lithium, respectively), the effective smoothing of the shell effects due to the rough surface is not expected to be strongly dependent on the element (for a given surface ionic structure). On the other hand, this does not hold true in respect of the supershell pattern, which is very sensitive to both the ratio A/R_{N_e} and the location of the Fermi level relative to the vacuum level.

Very large roughness amplitudes have been involved in this work ($A=3.5$ a.u.) and these might be considered as quite unphysical (this is undoubtedly true for small clusters). Nevertheless let us recall that this paper aims to report a systematic investigation of the corrugation effects, and that presently the actual cluster surface corrugation, which might depend on the experimental conditions prevailing during the cluster growth, cannot be estimated from "first-principles" calculations, especially for large clusters. Let us mention that a so-called "roughening transition," affecting planar surfaces or particle facets, is theoretically predicted to occur at finite temperature below the melting point.[48] This transition has been experimentally confirmed in the case of metal particles of micrometric size. This roughening transition has actually a statistical origin, and results from the counterbalancing of the increasing surface energy by entropy effects in the free energy (to a rough surface correspond much more atomic surface configurations). However, the extrapolation of such results to clusters of nanometric size is speculative, all the more that the observation of the JM-like electronic shell structure requires cluster temperatures consistent with the melting—or at least the surface melting—of the background.

ACKNOWLEDGMENTS

The authors acknowledge Nicolas Pavloff for sending his manuscript prior to publication. We thank the Region Rhône-Alpes for financial support in the frame of the plan Etat-Region. This work was also supported by the EC Contract No. CHRX-CT94-0612.

[1]W. D. Knight, K. Clemenger, W. A. de Heer, W. A. Saunders, M. Y. Chou, and M. L. Cohen, Phys. Rev. Lett. **52**, 2141 (1984).

[2]W. A. de Heer, Rev. Mod. Phys. **65**, 611 (1993), and references therein.

[3]M. Brack, Rev. Mod. Phys. **65**, 677 (1993), and references therein.

[4]J. Pedersen, S. Bjørnholm, J. Borgreen, K. Hansen, T. P. Martin, and H. D. Rasmussen, Nature **353**, 733 (1991).

[5]T. P. Martin, S. Bjørnholm, J. Borgreen, C. Bréchignac, Ph. Cahuzac, K. Hansen, and J. Pedersen, Chem. Phys. Lett. **186**, 53 (1991).

[6]M. Pellarin, B. Baguenard, C. Bordas, M. Broyer, J. Lermé, and J. L. Vialle, Phys. Rev. B **48**, 17 645 (1993).

[7]H. Ito, T. Sakurai, T. Matsuo, T. Ichihara, and I. Katakuse, Phys. Rev. B **48**, 4741 (1993).

[8]W. Ekardt, Phys. Rev. B **29**, 1558 (1984).

[9]D. E. Beck, Solid State Commun. **49**, 381 (1984).

[10]O. Genzken, M. Brack, E. Chabanat, and J. Meyer, Ber. Bunsenges. Phys. Chem. **96**, 1217 (1992).

[11]O. Genzken, Mod. Phys. Lett. B **7**, 197 (1993).

[12]C. Guet and W. R. Johnson, Phys. Rev. B **45**, 11 283 (1992).

[13]A. Rubio, L. C. Balbas, and J. A. Alonso, Z. Phys. D **19**, 93 (1991).

[14]G. Lauritsch, P. G. Reinhard, J. Meyer, and M. Brack, Phys. Lett. A **160**, 179 (1991).
[15]T. Hirschmann, M. Brack, and J. Meyer, Ann. Phys. (Leipzig) **3**, 336 (1994).
[16]J. Lermé, C. Bordas, M. Pellarin, B. Baguenard, J. L. Vialle, and M. Broyer, Phys. Rev. B **48**, 12 110 (1993).
[17]P. G. Reinhard, S. Weisgerber, O. Genzken, and M. Brack, in *Nuclear Physics Concepts in Atomic Cluster Physics,* edited by R. Schmidt, H. O. Lutz, and R. Dreizler (Springer-Verlag, Berlin, 1992).
[18]O. Genzken, P. G. Reinhard, M. Brack, H. Bresele, and G. Viling (unpublished).
[19]J. Lermé, M. Pellarin, B. Baguenard, C. Bordas, J. L. Vialle, and M. Broyer, Phys. Rev. B **50**, 5558 (1994).
[20]L. Serra, G. B. Bachelet, N. Van Giai, and E. Lipparini, Phys. Rev. B **48**, 14 708 (1993).
[21]S. A. Blundell and C. Guet, Z. Phys. D **33**, 153 (1995).
[22]J. Lermé, M. Pellarin, J. L. Vialle, and M. Broyer, Phys. Rev. B **52**, 2868 (1995).
[23]H. Nishioka, K. Hansen, and B. R. Mottelson, Phys. Rev. B **42**, 9377 (1990).
[24]U. Röthlisberger and W. Andreoni, J. Chem. Phys. **94**, 8129 (1991).
[25]V. Bonacic-Koutecky, P. Fantucci, and J. Koutecky, Chem. Rev. **91**, 1035 (1991).
[26]M. Manninen, Phys. Rev. B **34**, 6886 (1986).
[27]D. M. Lindsay, Y. Wang, and T. F. George, J. Chem. Phys. **86**, 3500 (1987).
[28]M. Manninen, J. Mansikka-aho, and E. Hammarén, Europhys. Lett. **15**, 423 (1991).
[29]J. Mansikka-aho, M. Manninen, and E. Hammarén, Z. Phys. D **21**, 271 (1991).
[30]M. Pellarin, E. Cottancin, B. Baguenard, J. Lermé, J. L. Vialle, and M. Broyer, Phys. Rev. B (to be published).
[31]K. F. Ratcliff, in *Multivariate Analysis V,* edited by P. R. Krishnaiah (North-Holland, Amsterdam, 1980).
[32]J. Barojas, E. Cota, E. Blaisten-Barojas, J. Flores, and P. A. Mello, Ann. Phys. **107**, 95 (1977).
[33]N. Pavloff (unpublished).
[34]J. P. Bucher, P. Xia, and A. Bloomfield, Phys. Rev. B **42**, 10 858 (1990).
[35]S. Tanaka and S. Sugano, Phys. Rev. B **34**, 740 (1986).
[36]U. Sivan and Y. Imry, Phys. Rev. B **35**, 6074 (1987).
[37]J. Mansikka-aho, M. Manninen, and E. Hammarén, Phys. Rev. B **47**, 10 675 (1993).
[38]J. Mansikka-aho, M. Manninen, and E. Hammarén, Z. Phys. D **31**, 253 (1994).
[39]N. Pavloff and M. S. Hansen, Z. Phys. D **24**, 57 (1992).
[40]W. P. Halperin, Rev. Mod. Phys. **58**, 533 (1986).
[41]T. A. Brody, J. Flores, J. B. French, P. A. Mello, A. Pandey, and S. S. M. Wong, Rev. Mod. Phys. **53**, 385 (1981).
[42]J. Mansikka-aho, E. Hammarén, and M. Manninen, Phys. Rev. B **46**, 12 649 (1992).
[43]R. Smoluchowski, Phys. Rev. **1**, 661 (1941).
[44]J. Lermé, C. Bordas, M. Pellarin, B. Baguenard, J. L. Vialle, and M. Broyer, Phys. Rev. B **48**, 9028 (1993).
[45]M. Brack, O. Genzken, and K. Hansen, Z. Phys. D **21**, 65 (1991).
[46]V. M. Strutinski, Nucl. Phys. A **122**, 1 (1968).
[47]M. Lombardi, P. Labastie, C. Bordas, and M. Broyer, J. Chem. Phys. **89**, 3479 (1988).
[48]M. C. Desjonquères and D. Spanjaard, in *Concepts in Surface Physics,* edited by R. Gomer, G. Ertl, and D. L. Mills (Springer-Verlag, Berlin, 1993).